HEFAT2014
10th International Conference on Heat Transfer, Fluid Mechanics and Thermodynamics
14–16 July 2014
Orlando, Florida

NUMERICALLY-BASED PARAMETRIC STUDY OF A COMPACT FIN-TUBE HEAT EXCHANGER

Jeanette Cobian-Iñiguez[1] **, Florian Dugast**[1,2]**, Arturo Pacheco-Vega**[1,*]
[1]Department of Mechanical Engineering
California State University at Los Angeles
Los Angeles, CA 90032, USA
E-mail: apacheco@calstatela.edu
[2]Department of Mechanical Engineering
Polytech' Nantes École D'Ingénieurs
Université de Nantes
Nantes Cedex 3, France

ABSTRACT

This study presents a comprehensive numerical analysis of the convective heat transfer on the external side of a compact fin-tube heat exchanger. The aim is to study the influence of key geometric parameters on both fluid flow and heat transfer processes in order to design more compact devices. The parameters are: fin spacing, tube diameter and tube alignment; i.e., in-line or staggered, for a set of typical operating conditions. The parametric analysis is established on a six-tube baseline heat exchanger model, where air flows over the tubes and water flows at high speed inside the tubes. The mathematical model of the convection process is comprised of the continuity, momentum and energy equations, in Cartesian coordinates, which is solved under specific flow and temperature values using the finite element method. From computed velocity, pressure and temperature fields, the values of heat rate and pressure drop are then calculated for a range of flow rates in the laminar regime. Results from this investigation indicate that tube diameter and fin spacing play a role in the amount of heat being exchanged and that, for a given device, the length needed to exchange 90% of the energy that could be achieved by the baseline model, is confined to less than 1/2 its actual size, and to exchange 98% of the associated thermal energy, less than 2/3 of its size is necessary.

NOMENCLATURE

A	[cm^2]	Cross sectional area
c_p	[J/kg·K]	Specific heat
D	[cm]	Tube diameter
k	[W/m·K]	Thermal conductivity
L	[cm]	Heat exchanger length
L_{x1}, L_{x2}	[cm]	Extended lengths
N		Number of tubes
Nu		Nusselt number
p	[Pa]	Pressure
Q	[W]	Heat rate
Q_T	[W]	Total heat rate
p	[Pa]	Pressure
T	[K]	Fluid temperature
T_s	[K]	Surface temperature
u, v, w	[cm/s]	Cartesian velocities
u_{in}	[cm/s]	Inlet velocity
x, y, z		Cartesian components
Special	characters	
ΔL	[mm]	Length of section
δ	[mm]	Fin spacing
ν	[m^2/s]	Kinematic viscosity
ρ	[kg/m^3]	Density

*Address all correspondence to this author.

Subscripts & superscripts	
$\overline{(\cdot)}$	average values
in	inlet
out	outlet

INTRODUCTION

Compact heat exchangers are widely used in industrial applications since they form an integral part of heating, cooling, ventilation and air conditioning systems (HVAC). In these thermal devices a common geometry is the plate-fin and tube configuration, where a hot fluid is usually driven inside tubes that are exposed to an external flow of a substance such as air at a lower temperature. Thermo-physical properties of air and the laminar nature of the flow in these systems cause the over-tube thermal resistance to critically constrain the transfer of energy, and to alleviate the problem the heat transfer area per unit volume is usually made very large. Thus, an important design objective for compact heat exchangers is to maximize device compactness while ensuring efficient heat transfer; in this way, operating and manufacturing costs can be significantly reduced while minimizing environmental impact.

Many studies have aimed at analyzing compact heat exchangers to enhance their performance. Romero-Mendez et al. [1] studied the effects of fin spacing on the air side of a single tube heat exchanger. They found that as fin spacing increased the flow not only would separate but also return towards the tube creating a strong recirculation. Motamedi et al. [2] numerically examined a 15-tube compact fin and tube heat exchanger with constant values of diameter and fin spacing, and showed that it was possible to achieve a dramatic reduction in device size. Erek et al. [3] conducted a numerical analysis on the effects of fin spacing, fin height, tube location and tube thickness on heat transfer and pressure drop in a fin and tube device by modeling only a segment of one tenth of the fin due to symmetric conditions. They reported that fin spacing affected pressure drop, confirming findings by others (c.f. [1]). Abu Madi et al. [4] analyzed the performance of heat exchangers with different fin-types via Colburn j- and friction f-factors. Their experiments show that the type of fin affected both heat transfer and friction factor, whilst f was not influenced by changes in number of tube-rows.

On the other hand, Jang et al. [5] used numerical analysis to study the effects of fin pitch, tube-row number and type of tube arrangement on the heat transfer rate of a multi-row heat exchanger via Nusselt numbers and pressure coefficients. Their results show that both average transfer coefficient and pressure drop are higher for staggered arrays than for in-line. A similar study was carried out by Tutar and Akkoca [6], with special emphasis on the transient effects of horseshoe vortex formation on heat transfer and pressure coefficients, reporting that such formation locally enhances both quantities. The effects of fin patterns on heat transfer and friction characteristics of multi-row fin and tube heat exchangers was experimentally studied by Tang et al. [7], whereas the unsteady turbulent flow effects in plate-fin and tube heat exchangers was studied by Zhang et al. [8] to analyze the effect of fin pitch. By using a logarithmic temperature difference between tube and fluid, it was found that Nusselt number increased with fin pitch. The influence of flow behavior, specifically horseshoe vortices, on heat transfer in a two-row tube and fin heat exchanger was studied by Tsai et al. [9] using topological theory and two-dimensional numerical simulations. Their findings confirm those of Zhang et al. [8] in that flow structure has a direct effect on the span-averaged Nusselt number and pressure drop, and heat transfer is enhanced by the helical nature of the horseshoe vortex.

In this study, we perform numerical simulations over plain-fin and tube heat exchangers and explore the heat transfer enhancement in these devices from a different angle; i.e., the increase in the efficacy of the system by identifying the regions in a complete device where most of the heat transfer takes place, and eliminating those that do not contribute significantly. We also propose to use the heat transfer rate instead of the common Nusselt number as the basis for the calculations, since it has been shown that this approach provides higher accuracy [10, 11]. The governing equations in Cartesian coordinates are first formulated and then solved on a representative computational domain by the finite element method. From the computed velocity, pressure and temperature fields, heat rates and pressure drops are then used to analyze the efficacy of the type of tube alignment and the effect of Reynolds number, fin spacing and diameter size. By comparing the solutions, for each case, to a baseline device, the length needed to exchange a specific fraction of the energy that would be transferred by the baseline model is finally computed.

PROBLEM DESCRIPTION

Consider the typical configuration of a plain-fin and tube compact heat exchanger in Figure 1. Air flows in direction of the arrows and cools the fluid flowing inside the tubes, the fins are separated a distance δ, L is the nominal length and H is its height. Regardless of the type of tube alignment, whether in-line or staggered, the heat exchanger under analysis has dimensions: $L = 38$ cm and $H = 44$ cm. The baseline values of fin spac-

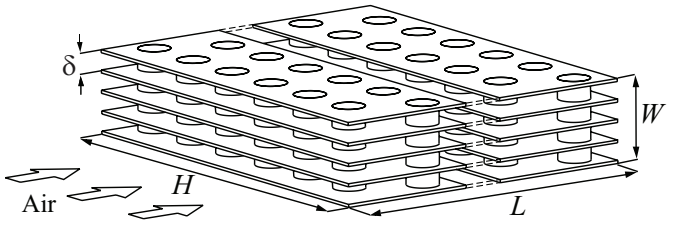

FIGURE 1. Schematic of a compact fin-tube heat exchanger.

ing and tube diameter, which will be used in a later section, are: $\delta_b \equiv \delta = 4.4$ mm and $D_b \equiv D = 31.8$ mm. Other dimensions are: the longitudinal fin pitch $P_l = 63.6$ mm, the center-tube distances to the leading and trailing edges $L_L = 68.2$ mm and $L_T = 68.2$ mm, and the transverse tube pitch $P_t = 63.6$ mm for in-line and $P_t = 31.8$ mm for staggered arrangements.

If we consider the incompressible flow of a Newtonian fluid, with constant properties, in the laminar regime, under steady-state conditions, and without body forces and viscous dissipation, the mathematical model is given by

$$\frac{\partial u}{\partial x} + \frac{\partial v}{\partial y} + \frac{\partial w}{\partial z} = 0, \tag{1}$$

$$u\frac{\partial u}{\partial x} + v\frac{\partial u}{\partial y} + w\frac{\partial u}{\partial z} = -\frac{1}{\rho}\frac{\partial p}{\partial x} + \nu\left(\frac{\partial^2 u}{\partial x^2} + \frac{\partial^2 u}{\partial y^2} + \frac{\partial^2 u}{\partial z^2}\right), \tag{2}$$

$$u\frac{\partial v}{\partial x} + v\frac{\partial v}{\partial y} + w\frac{\partial v}{\partial z} = -\frac{1}{\rho}\frac{\partial p}{\partial y} + \nu\left(\frac{\partial^2 v}{\partial x^2} + \frac{\partial^2 v}{\partial y^2} + \frac{\partial^2 v}{\partial z^2}\right), \tag{3}$$

$$u\frac{\partial w}{\partial x} + v\frac{\partial w}{\partial y} + w\frac{\partial w}{\partial z} = -\frac{1}{\rho}\frac{\partial p}{\partial z} + \nu\left(\frac{\partial^2 w}{\partial x^2} + \frac{\partial^2 w}{\partial y^2} + \frac{\partial^2 w}{\partial z^2}\right), \tag{4}$$

$$u\frac{\partial T}{\partial x} + v\frac{\partial T}{\partial y} + w\frac{\partial T}{\partial z} = \frac{k}{\rho c_p}\left(\frac{\partial^2 T}{\partial x^2} + \frac{\partial^2 T}{\partial y^2} + \frac{\partial^2 T}{\partial z^2}\right), \tag{5}$$

where, for air, the density is $\rho = 1.193$ kg/m^3, the dynamic viscosity $\nu = \mu/\rho = 1.52 \times 10^{-5}$ m^2/s, the specific heat $c_p = 1007$ J/kg·K, and the thermal conductivity $k = 0.0257$ W/K·m. The boundary conditions are: non-slip impermeable walls, symmetry at the mid-plane $z = 0$ and at those constant-y planes where the condition naturally arises; i.e., $y = 0$ and $y = P_t/2$, uniform flow at the inlet and fully developed flow at the outlet, plus uniform inlet temperature, isothermal walls and zero temperature gradients at the outlet. It is important to note that considering a conjugate version of this problem could slightly improve the calculations; however, it has been shown that the difference between ideal and real fins is usually small [12], and most calculations reported in the literature have used the isothermal-wall assumption without significantly degrading the accuracy of the results.

A schematic of the computational domain for both configurations is shown in Figure 2, where it can be seen that two additional sections; named, L_{x1} and L_{x2}, extend from the actual heat exchanger domain to enforce, with high accuracy, the inlet and outlet conditions, as demonstrated by Jang et al. [5] and Romero-Mendez et al. [1]. Importantly, the actual values of L_{x1} and L_{x2} depend on the operating conditions and the heat tube configuration, and are computed via an iterative process. Starting with very large values for both quantities, one of them is fixed while the other is decreased. The streamwise velocity at specific locations in the leading edge for L_{x1} and trailing edge for L_{x2}, is used as control parameter. The minimum length corresponds to the last value for which u is less than a preset tolerance of 2 % with respect to the velocity computed with the initial values of

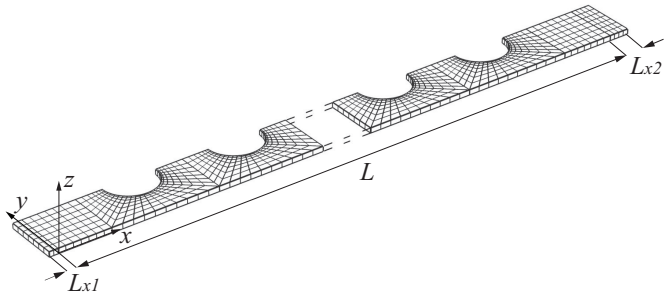

(a) In-line alignment.

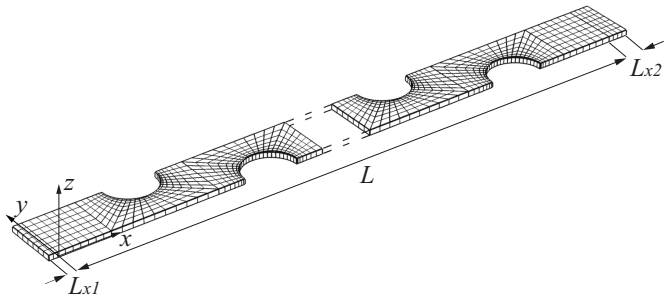

(b) Staggered alignment.

FIGURE 2. Schematic of the type of mesh used in the computational domain.

the extended lengths. Once the value of one of the quantities is computed, the process is carried out for the other. For the baseline configuration and $Re = 960$, which corresponds to the upper bound for the flowrate, $L_{x1} = 20$ mm and $L_{x2} = 14$ mm.

NUMERICAL TECHNIQUE

The governing equations (1)–(5) were discretized on the computational domain and solved by the finite element method. Although other numerical techniques, like those based on finite differences have been developed [13], and successfully applied to a number of fluid flow and heat transfer problems [14]– [16], the main advantage of the finite element method is its treatment of the boundary conditions on curved surfaces.

The problem under analysis was solved using the general-purpose finite-element software COMSOL Multiphysics (http://www.comsol.com). Here, the computational domain is discretized using a three-dimensional mesh; with hexahedral elements being applied in it, and quadrilateral elements along the boundaries. The degrees of freedom for temperature, velocity and pressure are all assigned at the nodes of the elements. To ensure accurate results while maintaining a manageable CPU time, more dense meshing is using near all the walls. Schematics of a typical discretization domain for both tube alignments are shown in Figure 2 where, for each section, 72 elements are evenly dis-

tributed around the tube perimeter and mapped outward in a radial fashion to the outer edges of the section, and subsequently linked to a regular mapped mesh. A total of 48,585 and 54,704 elements were used, respectively, in the in-line and staggered arrangements; the difference being associated with the slightly larger L_{x2} for the staggered geometry. In both cases, the element sizes close to the walls were chosen sufficiently small to be able to resolve the boundary layers. The velocity and temperature fields were computed from the resulting system of algebraic equations by the generalized minimum residual (GMRES) iterative solver, for which the relative tolerance was set to 10^{-6}.

To ensure grid independence of the numerical results, several grids were tested for different values of inlet velocity (i.e., Reynolds numbers). These tests were done for pressure p, streamwise velocity u and temperature T, at a fixed point in the domain of both in-line and staggered configurations. It was found that regardless of the tube arrangement, a grid with at least 48,000 elements is sufficient to achieve an accuracy within 2% of the results obtained with a grid containing 1,823,493 elements, while maintaining a manageable CPU time.

RESULTS AND DISCUSSION

The parametric analysis conducted here focuses on the effects of Reynolds number Re, fin spacing δ, tube diameter D and tube configuration. Although Motamedi et al. [2] used a definition of Re based on diameter $Re_D = u_{in}D/\nu$ to study effects of Re and temperature difference between inlet fluid and the walls, $\Delta T = T_s - T_{in}$, in a 15-tube compact heat exchanger, due to the fact that here tube diameter and fin spacing are varied, in addition to Re_D we also use a Reynolds number based on fin spacing $Re_\delta = u_{in}\delta/\nu$, as suggested by Romero-Mendez et al. [1]. However, we only consider a value $\Delta T = 20$, K with $T_s = 313$ K and $T_{in} \equiv \overline{T}_{in} = 293$ K. The corresponding ranges for Reynolds numbers are: $Re_D \in [120, 960]$ and $Re_\delta \in [16, 134]$ with $Re_\delta = (\delta/D)Re_D$ providing the equivalence between the two definitions. To simplify the analysis, we consider baseline values of fin spacing and tube diameter as D_b and δ_b, so that $\delta = \{0.5, 1\}\delta_b$ mm and $D = \{0.25, 0.5, 0.75\}D_b$ mm, respectively. Recall that $D_b = 31.8$ mm and $\delta_b = 4.4$ mm.

Following Motamedi et al. [2], results for pressure, streamwise flow velocity and temperature presented here are based on average values given as

$$\overline{p} = \frac{1}{A}\int_A p\, dA, \tag{6}$$

$$\overline{u} = \frac{1}{A}\int_A (\mathbf{u}\cdot\mathbf{n})\, dA, \tag{7}$$

$$\overline{T} = \frac{\int_A (\mathbf{u}T\cdot\mathbf{n})\, dA}{\int_A (\mathbf{u}\cdot\mathbf{n})\, dA}. \tag{8}$$

In the equations above, A is the local cross-sectional area normal to the unit vector $\mathbf{n}$ associated with the surface of interest $dA = dy\, dz$, and hence perpendicular to the streamwise direction of the flow at any point along x, while $\mathbf{u}$, T and p are the local values of the velocity vector, temperature and pressure. Energy balances at each section, and between inlet and outlet of the heat exchanger, provide, respectively, the so-called *partial*, Q_j, and total, Q_T, heat rates, which can be quantified by

$$Q_j = \rho\overline{u}\, Ac_p \left[\, \overline{T}(x_{j-1}) - \overline{T}(x_j)\right], \tag{9}$$

where $x_{j-1} = x((j-1)\cdot\Delta L)$ and $x_j = x(j\cdot\Delta L)$, for $j = 1, ..., 6$, represent the location of the inlet and outlet planes of the j-th section, and

$$Q_T = \sum_{j=1}^{6} Q_j + Q_{L_{x1}} = \rho\overline{u}\, Ac_p(\overline{T}_{out} - \overline{T}_{in}), \tag{10}$$

where $\overline{T}_{in}$ and $\overline{T}_{out}$ are the average temperatures at the inlet and outlet planes of the entire computational domain for the device. Note that $Q_{L_{x1}}$ in Eq. (10) is the energy transferred by the combined effect of advection and diffusion to/from the fluid that occurs as the fluid approaches the leading edge of the heat exchanger, and before the fluid interacts with the actual surfaces, due to temperature gradients along the streamwise direction.

On the other hand, the term ΔL above is the length of a specific section of the device that may be selected by the thermal engineer. It is important to note that in this work we propose the use of the heat rate instead of averaged Nu numbers. We believe that this approach provides higher accuracy since a characteristic temperature difference is not needed [10, 11], although it may come at the expense of more generality. As mentioned before, the baseline heat exchanger has $N = 6$ tubes in the streamwise direction.

Hydrodynamics and Heat Transfer

Typical velocity and temperature fields are represented qualitatively by streamlines, isotherms and temperature contours at the mid-plane $z = \delta/2$, for $Re_D = 480$ and $\delta = 4.4$ mm, in Figure 3 for the in-line configuration, and in Figure 4 for the staggered arrangement. From Figures 3(a) and 4(a) it can be seen that the flow is nearly uniform at the inlet, develops throughout the heat exchanger length into a periodic one with recirculation regions behind the tubes, as expected for this value of Re. This periodicity is broken at the outlet. A main difference between the in-line and staggered flow patterns is that the latter alternate due to the tube arrangement affecting the heat transfer process. It is worth noting that similar flow behavior was observed for $Re = 960$; while at low flow velocities, e.g., $Re = 120$ and $Re = 240$, though periodic, the flow does not show any recirculation.

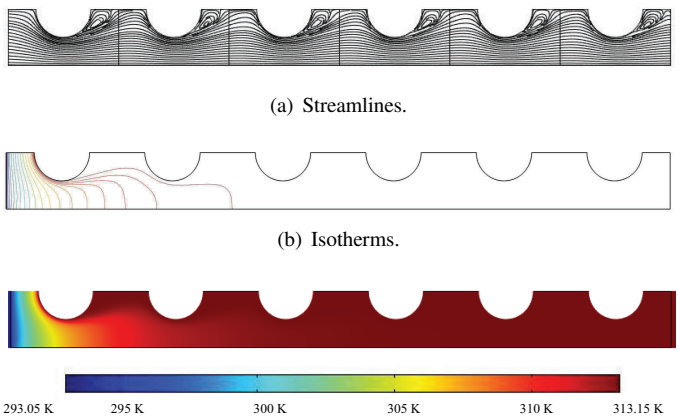

(a) Streamlines.

(b) Isotherms.

(c) Temperature contours.

FIGURE 3. Streamlines, isotherms and temperature contours for in-line configuration, $Re_D = 480$, $\delta = \delta_b = 4.4$ mm.

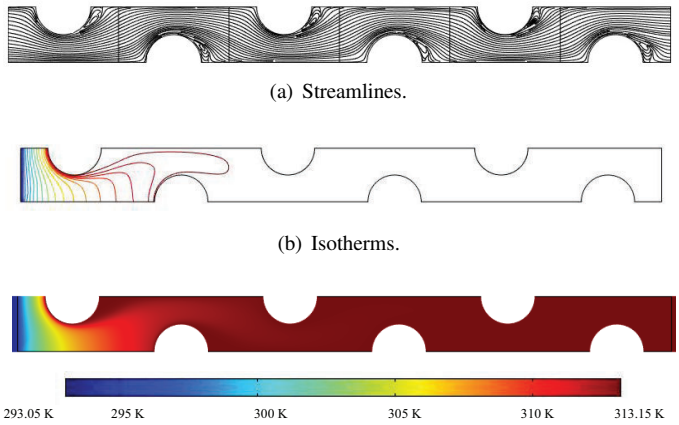

(a) Streamlines.

(b) Isotherms.

(c) Temperature Countours.

FIGURE 4. Streamlines, isotherms and temperature contours for staggered configuration, $Re_D = 480$, $\delta = \delta_b = 4.4$ mm.

It is important to note that because at high Re numbers (e.g., $Re = 960$), unsteady flow patterns are expected, to ensure that our steady-state model provides accurate results, though not shown here for brevity, we have also carried out time dependent analyses for all Re numbers considered in this study. The corresponding results indicate that with exception of $Re = 960$, for all other values of Re the flow was steady. However, even in the case of $Re = 960$, unsteady flow patterns appear only at the trailing edge of the heat exchanger and thus do not have any effect on the flow patterns and/or temperature profiles in the device.

The relationship between energy transfer and hydrodynamics shown in Figures 3(c) and 3(b) for in-line and Figures 4(b) and 4(c) for staggered tube alignment indicate that the arrangement plays a role as the thermal energy is advected downstream in a slightly different fashion, with the isotherms illustrating this fact. Common to both geometries is that most of the temperature change is achieved in the first and second tubes. Furthermore, a fact more clearly distinguished from the temperature contours is that for both configurations the total heat transfer has occurred just before the flow reaches the third tube.

Finally, as mentioned before, energy transfer starts to occur before the fluid enters in contact with the actual surfaces. Thus, due to this fact, in the next sections it will be shown that the value of fluid temperature at the leading edge of the device is always higher than that at the inlet boundary condition, and therefore the value of $\sum_j Q_j/Q_T$; i.e., the energy transferred in the actual device, is always less than 1. Importantly, the deficit in Q; i.e., $Q_{L_{x1}}$, depends strongly on Re.

Reynolds Number Effect

We analyze the Reynolds number effect on the heat transfer of the base heat exchanger with $D = D_b$ and $\delta = \delta_b$; the same trend was found in all the other models considered. Figures 5 and 6 show the average temperature at several cross-sections along the heat exchanger length for both in-line and staggered configurations, respectively. From Figure 5 it can be seen that due to the convective process of thermal energy, the temperature increases until reaching the value of the surface temperature of fins and tubes. However, differences are noticeable in the location at which this upper bound value is reached. For small Re (i.e. $Re = 120$ and 240), T_s is reached close to the inlet heat exchanger, whereas for larger inlet velocities (i.e. $Re = 480$ and 960) a large proportion of the device is required to reach it. From the average temperature distribution, the corresponding heat rate can be obtained from Eq. (9), it can be seen that at low Re the total heat rate occurs within the first 1/3 of the total length L, while for $Re = 960$, 90% of the device length is necessary to transfer the total amount of energy.

On the other hand, temperature distributions shown in Figure 6 for the staggered alignment exhibit similar trends as that for the in-line configuration. Again, the temperature increases until reaching the value surface temperature at different x-locations. For small Re, this temperature is reached close to the inlet of the device, whereas for larger Re, T_s is reached close to the outlet. The locations at which the total transfer of energy corresponding to small and large Re numbers coincide with those of the in-line heat exchanger.

It is important to note that, as indicated in the previous sections, in both configurations energy transfer to air starts to take place before it actually reaches the leading edge of the heat exchanger due to advection and diffusion of energy, as shown in Figures 5 and 6 from the increased values in temperature at the leading edge $x = 0$ which are all different from that at the inlet boundary of the computational domain. The flow velocity decreases due to the presence of the fins and tubes and heat transfer

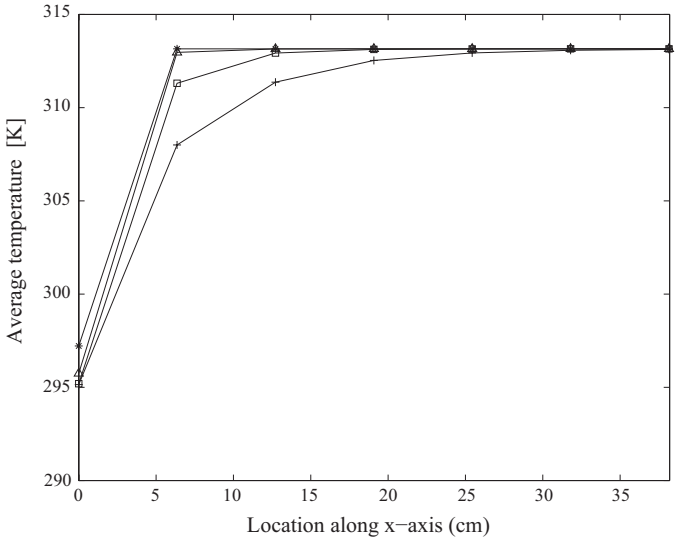

FIGURE 5. Temperature distribution for different Reynolds numbers; in-line configuration. $-*-$ $Re = 120$; $-\triangle-$ $Re = 240$; $-\square-$ $Re = 480$; $-+-$ $Re = 960$.

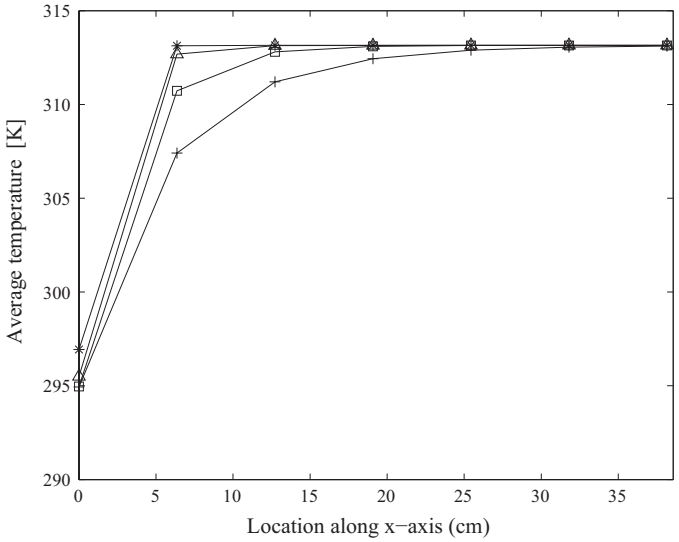

FIGURE 6. Temperature distribution for different Reynolds numbers; staggered configuration. $-*-$ $Re = 120$; $-\triangle-$ $Re = 240$; $-\square-$ $Re = 480$; $-+-$ $Re = 960$.

by diffusion becomes significant, particularly at low Re numbers in which the residence time is larger. Since the aforementioned effects are quantified by the term $Q_{L_{x1}} = \dot{m}c_p\left[\overline{T}(x_0) - \overline{T}_{in}\right]$, the values of $Q_{L_{x1}}/Q_T$ for the in-line configuration are 22.5 % for $Re = 120$, and decrease as Re increases; e.g., 12 % for $Re = 240$, 7 % for $Re = 480$, slightly increasing again to 8.9 % for $Re = 960$. Similar numbers were obtained for the staggered arrangement.

Tube Diameter Effect

The effects of varying the tube diameter on fluid flow and energy transfer were studied for both configurations, several Reynolds numbers and a set of four diameter sizes $\{D = 0.25, 0.5, 0.75, 1\} \cdot D_b$. The heat transfer rate is presented in terms of the ratio Q/Q_T; i.e., the fraction of total heat rate that could be achieved from a corresponding baseline device; the pressure drop $\Delta\overline{p}$ is used for the hydrodynamics.

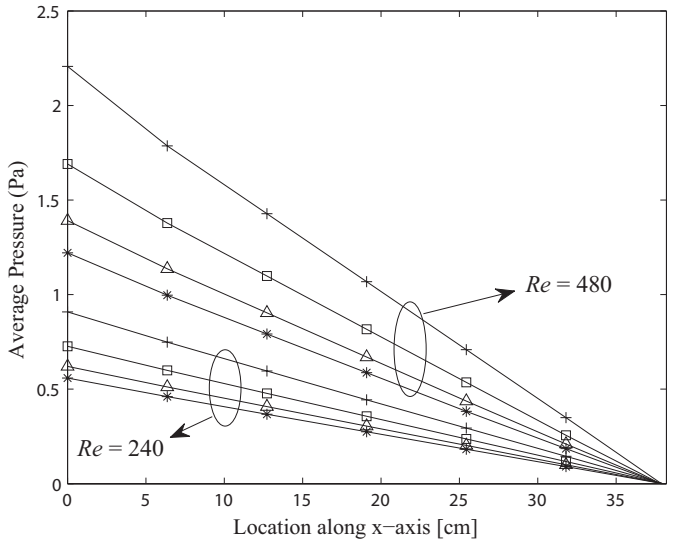

FIGURE 7. Average pressure for $\delta = 4.4$ mm and different diameters for In-line configuration. $-*-$ $D = 0.25D_b$; $-\triangle-$ $D = 0.5D_b$; $-\square-$ $D = 0.75D_b$; $-+-$ $D = D_b$.

Figure 7 depicts the average pressure at different sections of the heat exchanger length for the in-line case, whereas the staggered case is shown in Figure 8. Two Re numbers, $Re = 240$ and $Re = 480$, are shown as examples, the same trend being found for $Re = 120$ and 960. From both figures it can be observed that, as expected, higher Re values (larger inlet velocities) provide higher pressure drops. By focusing on the effect of diameter variation, on the other hand, it is clearly seen that for both configurations, as diameter decreases so does pressure drop, since small diameters reduce blockage on the flow. In general, and expected, the staggered arrangement gives rise to slightly larger pressure drops.

In order to find whether a smaller device would be able to transfer the inherent thermal energy of a baseline heat exchanger, the heat transfer ratio was calculated at each tube section. Although we performed numerical simulations for $Re = \{120, 240, 480, 960\}$, with a fixed fin spacing of $\delta = \delta_b = 4$ mm,

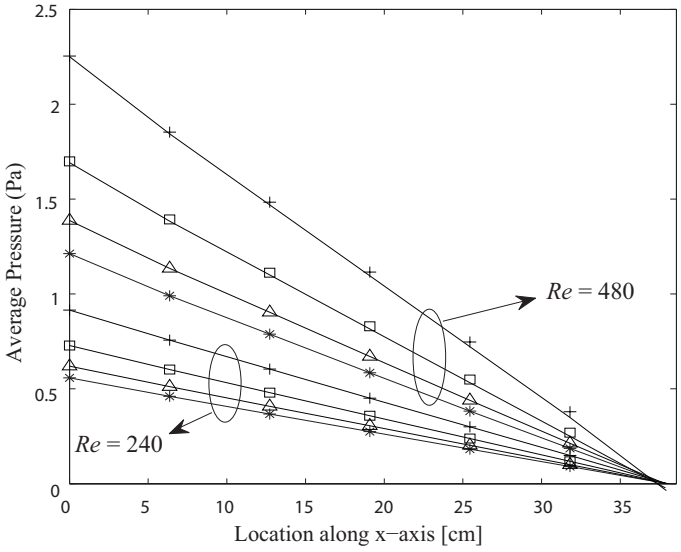

FIGURE 8. Average pressure for $\delta = 4.4$ mm and different diameters for staggered configuration. $-*-$ $D = 0.25D_b$; $-\triangle-$ $D = 0.5D_b$; $-\square-$ $D = 0.75D_b$; $-+-$ $D = D_b$.

in Figures 9 and 10 we highlight results for $Re = 240$ and 480 as the other Re-values considered yielded similar results. At low Reynolds numbers, it was found that most of the heat transfer occurred again closer to the inlet. For $Re = 240$ for example, 80% of the total heat transferred to the fluid occurred at tube section one, whereas for $Re = 480$ the value ranges at 70-76%, and as can be observed in both Figures 9 and 10, 98% of the total energy transfer was completed after the second tube section; the rest of the device did not contribute significantly. From Figures 9(a) and 10(a) it can also be seen that at low Reynolds numbers ($Re = 120$ and 240) tube diameter variations do not affect the heat transfer as Q/Q_T remained nearly equivalent at each tube section.

At increased inlet velocities however, heat transfer was indeed affected by tube diameter. From Figures 9(b) and 10(b) it can be observed that as tube diameter decreases the heat rate at a section increases. A device with a diameter D equal to the baseline D_b, in tube section 1 the value of Q/Q_T was approximately 70%, whereas one with $D = 0.25D_b$ such ratio increased to nearly 77%. Though not shown here, similar behavior was observed for $Re = 960$. Thus, as flow velocity increases, the effects of tube diameter on heat transfer will increase.

As indicated above, devices operating at higher Reynolds numbers require a larger number of sections for the fluid to attain the value of the surface temperature due to less residence time at each section. In consequence, the ratio of heat transferred in the first tube section with respect to the total amount that could be potentially exchanged by an associated baseline device decreases

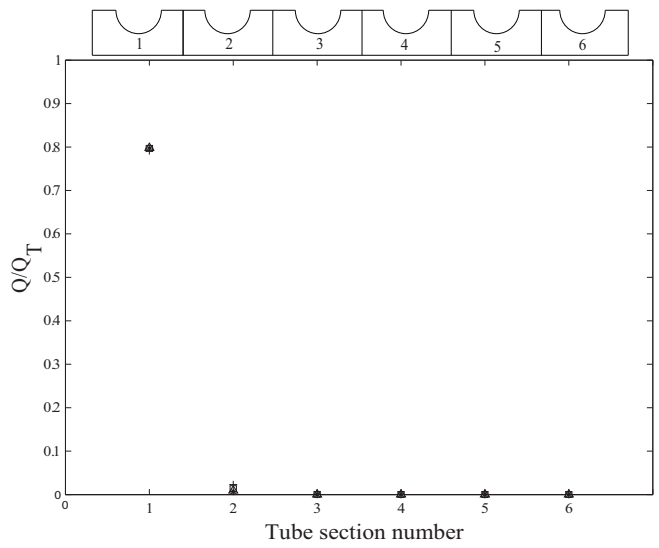

(a) $Re = 240$.

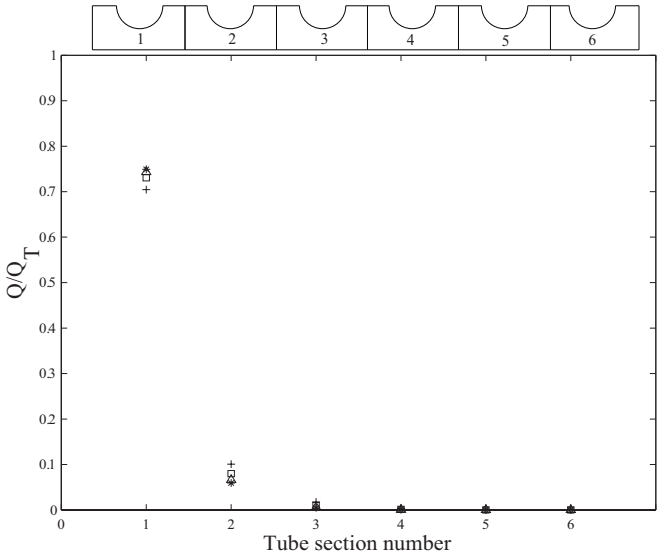

(b) $Re = 480$.

FIGURE 9. Fraction of heat rate Q/Q_T for in-line configuration, $\delta = 4.4$ mm and different values of D. $-*-$ $D = 0.25D_b$; $-\triangle-$ $D = 0.5D_b$; $-\square-$ $D = 0.75D_b$; $-+-$ $D = D_b$.

in comparison to the case of a device operating at a lower Re value. Conversely, the trend reverses for the other sections. In addition, it is clear that the total energy transferred (in W) by the device with the larger Re-flow is higher. Finally, heat transfer ratio and temperature distributions exhibited a similar trends in both the staggered and in-line arrangements, and as seen from the results, no major differences for heat rate exist between in-line and staggered configurations.

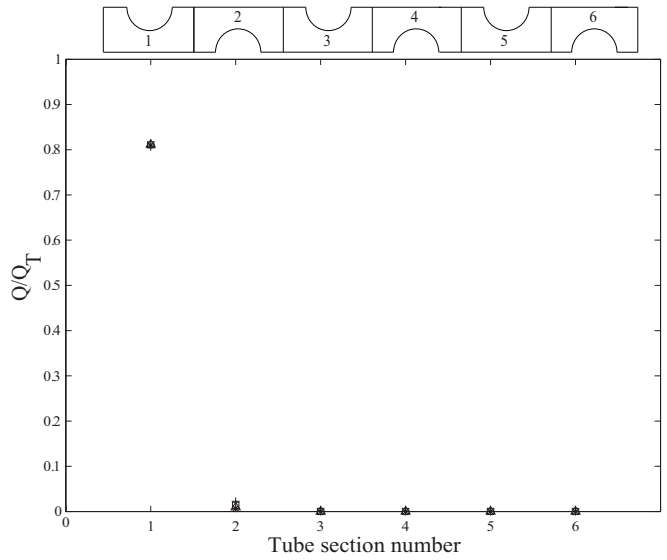

(a) $Re = 240$.

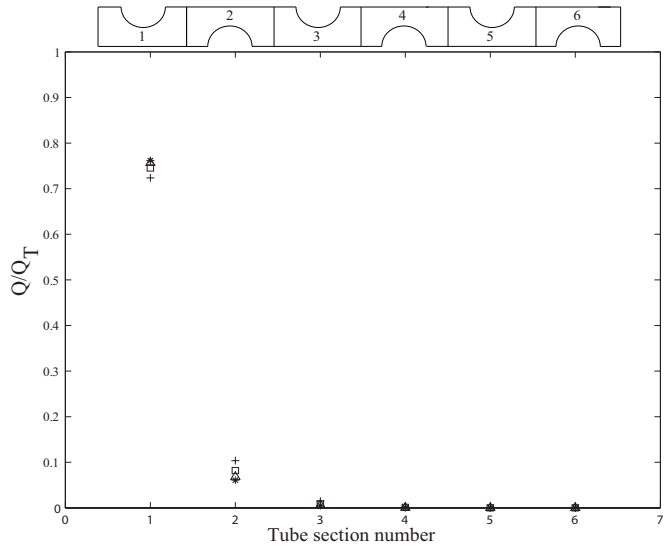

(b) $Re = 480$.

FIGURE 10. Fraction of heat rate Q/Q_T for staggered configuration, $\delta = 4.4$ mm and different values of D. $-*-$ $D = 0.25D_b$; $-\triangle-$ $D = 0.5D_b$; $-\square-$ $D = 0.75D_b$; $-+-$ $D = D_b$.

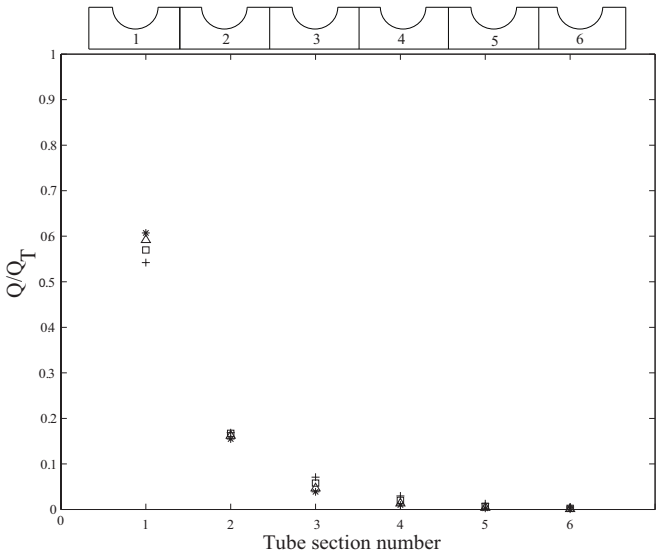

(a) $\delta = 4.4$ mm.

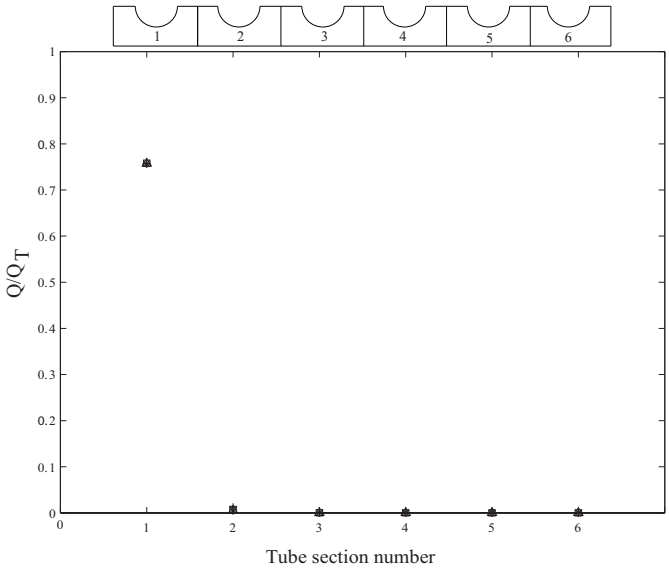

(b) $\delta = 2.2$ mm.

FIGURE 11. Fraction of heat rate Q/Q_T for in-line configuration, $Re = 960$ and different values of D. $-*-$ $D = 0.25D_b$; $-\triangle-$ $D = 0.5D_b$; $-\square-$ $D = 0.75D_b$; $-+-$ $D = D_b$.

Fin Spacing Effect

The effects of varying fin spacing were assessed by using two values of it: the baseline fin spacing $\delta = \delta_b = 4.4$ mm and a value half of it $\delta = \delta_b/2 = 2.2$ mm. Since all the results in the previous sections were obtained with the value of $\delta = 4.4$ mm, for *Re* numbers of 240 and 480, in the present case we have focused on $Re = 960$ which is the limiting case. Figures 11(a) and 11(b) show, respectively, the fraction of energy transferred at each section of the device with $\delta = 4.4$ mm and $\delta = 2.2$ mm, for the in-line arrangement, whereas Figures 12(a) and 12(b) show the corresponding results for the staggered alignment. From the figures it can be seen that for a fixed *Re* number, and regardless of the tube arrangement, the effect of reducing the fin spacing is essentially the same as that of reducing the value of *Re* for a fixed δ. For instance, devices with larger fin spacings (there is a limit as reported by Romero-Mendez et al. [1]) require a larger

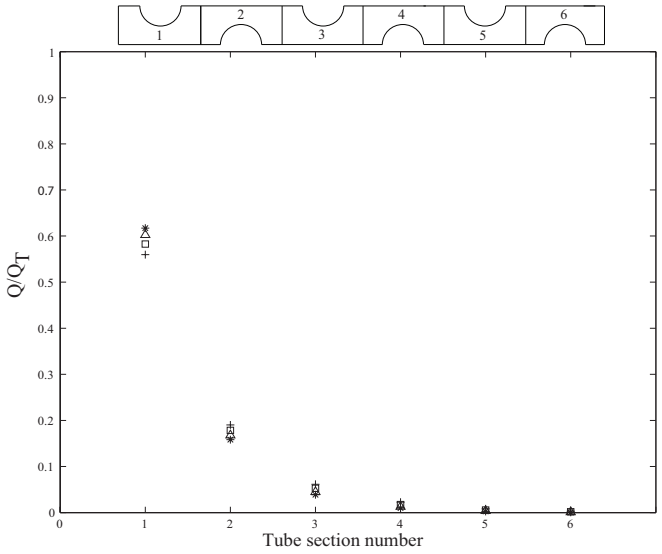

(a) $\delta = 4.4$ mm.

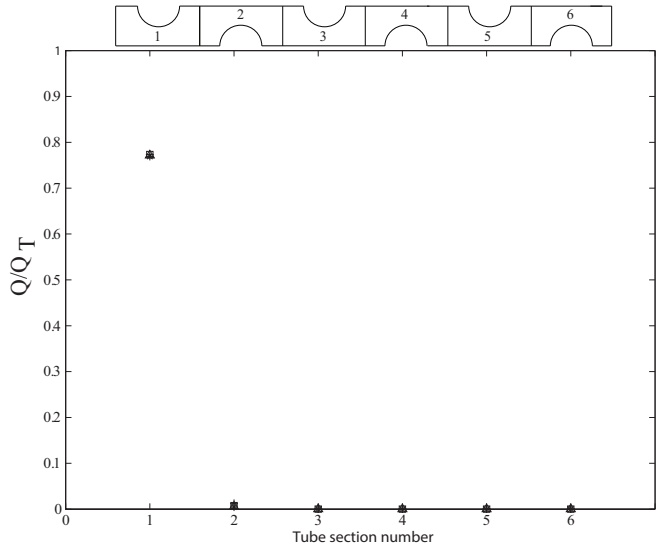

(b) $\delta = 2.2$ mm.

FIGURE 12. Fraction of heat rate Q/Q_T for staggered configuration, $Re = 960$ and different values of D. $-*-$ $D = 0.25D_b$; $-\triangle-$ $D = 0.5D_b$; $-\square-$ $D = 0.75D_b$; $-+-$ $D = D_b$.

number of sections for the fluid to attain the value of the surface temperature due to larger amount of fluid mass at each section. For instance, with $\delta = 4.4$ mm, a minimum of four tubes were required to achieve 99% of total possible heat transfer. By reducing the fin spacing to $\delta = 2.2$ mm, the total amount of tube sections required to complete the possible energy transfer of an associated baseline device was reduced to only two. Furthermore, it was observed that decreasing the fin spacing enabled to reduce the effect of tube diameter on the heat transfer.

CONCLUSIONS

In this study we have analyzed the hydrodynamic and heat transfer characteristics of compact fin and tube heat exchangers. We found that factors such as tube diameter, fin spacing, Reynolds number and tube alignment influence the transfer of energy. A device with air flowing at $Re = 240$, e.g., reached the surface temperature much closer to the inlet than a device with air flowing at $Re = 480$. Furthermore, variation of tube diameter showed that this parameter affects heat transfer and pressure drop for high *Re* numbers. Decreasing the tube diameter increased the relative energy transfered near the inlet. Similarly, decreasing fin spacing increased the fraction of thermal energy transfered in the first tube sections; small fin spacing allows less fluid mass to pass through the heat exchanger. It can be argued from the results in this study that when designing a more compact fin and tube heat exchanger that will reduce energy required for operation and manufacturing, parameters such as fin spacing, tube diameter and flow velocity should be analyzed in conjunction. System optimization, in which the interactions between the parameters are included, will be carried out using genetic algorithms and will be reported in the future.

ACKNOWLEDGMENT

Jeanette Cobian-Iñiguez is the recipient of a LSAMP fellowship funded by NSF HRD-1246662 for which we are grateful. Florian Dugast thanks financial support from CEaS-CSULA for a summer internship. Comments from an anonymous referee greatly helped improve the paper and are much appreciated. This project has been partially supported by NSF grants HRD-0932421 and ARA-R2-0963539.

REFERENCES

[1] Romero-Mendez, R., Sen, M., Yang, K., and McClain, R., 2000. "Effect of fin spacing on convection in a plate fin and tube heat exchanger". *Int. J. Heat and Mass Transfer,* ***43***, pp. 39–51.

[2] Motamedi, A., Pacheco-Vega, A., and Pacheco, J., 2012. "Numerical analysis of a multi-row multi-column compact heat exchanger". *Journal of Physics: Conference Series,* ***395***, Paper 012121, pp. 1–9.

[3] Erek, A., Ozerdem, B., Billir, L., and Ilker, Z., 2005. "Effect of geometric parameters on heat transfer and pressure drop characteristics of plate fin and tube heat exchangers". *Applied Thermal Engineering,* ***25***, pp. 2421–2431.

[4] Abu Madi, M., Johns, R., and Heikal, M., 1998. "Performance characteristics correlation for round tube and plate finned heat exchangers". *Int. J. Refrigeration.,* ***21***(7), pp. 507–517.

[5] Jang, J.-Y., Wu, M.-C., and Chang, W., 1996. "Numerical en experimental studies of three dimensional plate-fin and

tube heat exchangers". *Int. J. Heat and Mass Transfer,* ***39***, pp. 3057–3066.

[6] Tutar, M., and Akkoca, A., 2004. "Numerical analysis of fluid flow and heat transfer characteristics in three-dimensional plate fin-and-tube heat exchangers". *Numer. Heat Transfer, Part A,* ***46***, pp. 301–321.

[7] Tang, L., Min, Z., Xie, G., and Wang, Q., 2009. "Fin pattern effects on air-side heat transfer and friction characteristics of fin-and-tube heat exchangers with large number of large-diameter tube rows". *Heat Transfer Engineering,* ***30***(3), pp. 171–180.

[8] Zhang, L.-Z., Zhong, W.-C., Chen, J.-M., and Zhou, J.-R., 2011. "Fluid flow and heat transfer in plate-fin and tube heat exchangers in a transitional flow regime". *Numer. Heat Transfer, Part A,* ***60***, pp. 766–784.

[9] Tsai, S., Tony, W., and Sheu, H., 1998. "Some physical insights into a two-row finned tube heat transfer". *J. Computers and Fluids,* ***27***(1), pp. 29–46.

[10] Pacheco-Vega, A., Díaz, G., Sen, M., Yang, K., and McClain, R., 2001. "Heat rate predictions in humid air-water heat exchangers using correlations and neural networks". *ASME J. Heat Transfer,* ***123***(2), pp. 348–354.

[11] Pacheco-Vega, A., Sen, M., and Yang, K., 2003. "Simultaneous determination of in- and over-tube heat transfer correlations in heat exchangers by global regression". *Int. J. Heat and Mass Transfer,* ***46***(6), pp. 1029–1040.

[12] R., R.-M., R., A., and M., S., 2001. "Study of the parameters affecting conjugated heat transfer in plate-fin and tube heat exchanger". *Interciencia,* ***26***(8), pp. 321–326.

[13] Pacheco, J. R., 2001. "The solution of viscous incompressible jet flows using non-staggered boundary fitted coordinate methods". *Int. J. Numer. Methods Fluids,* ***35***, pp. 71–91.

[14] Pacheco, J., and Pacheco-Vega, A., 2003. "Analysis of thin film flows using a flux vector splitting". *J. Fluids Engineering.,* ***125***, pp. 365–374.

[15] Pacheco, J., Pacheco-Vega, A., Rodić, T., and Peck, R., 2005. "Numerical simulations of heat transfer and fluid flow problems using an immersed-boundary finite-volume method on non-staggered grids". *Numer. Heat Transfer, Part B,* ***48***, pp. 1–24.

[16] Pacheco-Vega, A., Pacheco, J., and Rodić, T., 2007. "A general scheme for the boundary conditions in convective and diffusive heat transfer with immersed boundary methods". *ASME J. Heat Transfer,* ***129***, pp. 1506–1516.